OPEN ACCESS
IOP Publishing
Nanotechnology
Nanotechnology **34** (2023) 505714 (13pp)
https://doi.org/10.1088/1361-6528/acf8ce

Simultaneous quantification of Young's modulus and dispersion forces with nanoscale spatial resolution

Clodomiro Cafolla[1,*], **Kislon Voïtchovsky**[1] and **Amir Farokh Payam**[2,*]

[1] Physics Department, Durham University, Durham, DH1 3LE, United Kingdom
[2] Nanotechnology and Integrated Bioengineering Centre (NIBEC), School of Engineering, Ulster University, United Kingdom

E-mail: clodomiro.cafolla@durham.ac.uk and a.farokh-payam@ulster.ac.uk

Received 7 June 2023, revised 4 September 2023
Accepted for publication 11 September 2023
Published 11 October 2023

Abstract

Many advances in polymers and layered materials rely on a precise understanding of the local interactions between adjacent molecular or atomic layers. Quantifying dispersion forces at the nanoscale is particularly challenging with existing methods often time consuming, destructive, relying on surface averaging or requiring bespoke equipment. Here, we present a non-invasive method able to quantify the local mechanical and dispersion properties of a given sample with nanometer lateral precision. The method, based on atomic force microscopy (AFM), uses the frequency shift of a vibrating AFM cantilever in combination with established contact mechanics models to simultaneously derive the Hamaker constant and the effective Young's modulus at a given sample location. The derived Hamaker constant and Young's modulus represent an average over a small (typically <100) number of molecules or atoms. The oscillation amplitude of the vibrating AFM probe is used to select the length-scale of the features to analyse, with small vibrations able to resolve the contribution of sub-nanometric defects and large ones exploring effectively homogeneous areas. The accuracy of the method is validated on a range of 2D materials in air and water as well as on polymer thin films. We also provide the first experimental measurements of the Hamaker constant of HBN, MoT_2, WSe_2 and polymer films, verifying theoretical predictions and computer simulations. The simplicity and robustness of the method, implemented with a commercial AFM, may support a broad range of technological applications in the growing field of polymers and nanostructured materials where a fine control of the van der Waals interactions is crucial to tune their properties.

Supplementary material for this article is available online

Keywords: materials characterisation, AFM in air and liquid, elastic and dispersive forces at the nanoscale

(Some figures may appear in colour only in the online journal)

Introduction

Quantification of the physical and chemical properties of interfaces at the nanoscale is of crucial importance in the development of new materials with tailored features [1–5]. This is, for example, the case for two-dimensional (2D) materials and van der Waals (vdW) heterogenous structures where a molecular-level understanding of the interactions at

* Authors to whom any correspondence should be addressed.

play is key to achieve the desired physical, chemical and electronic properties [4–8]. With building units as thin as a single atomic layer, 2D materials tend to exhibit properties dissimilar from their bulk counterpart and can be dramatically influenced by any interactions with a contacting material [1, 9]. These unique features open a wealth of opportunities for the new generation of electronic devices, combining direct access to high mobility charge carriers and high thermal conductivity [1]. A plethora of exciting properties further arises when combining 2D materials in a single stack or when depositing them on different substrates [1, 10, 11]. Examples range from extending the plasmonic response of devices in the visible range [12] to developing ferromagnetic semiconductors [10, 12] and superlubricity in tribology and lubrication [13].

Fabricating these new 2D materials by design is however challenging [1, 14, 15]. Undesired structural defects can detrimentally alter the electronic and nanomechanical properties of 2D materials: wrinkles and ripples in mechanically exfoliated MoS_2, or graphene nanobubbles can modify the carrier concentration [16]. Alongside chemical and physical singularities, the other limiting factor in the effective design of 2D materials is the difficulty to fine control the interfacial interactions between each layer, and with the substrate [17]. The structure and properties of a given 2D device typically depend on a balance between vdW adhesion forces and the material's bending energy. In MoS_2, for example, interfacial defects lead to an increase in tensile strain with an associated transition from direct to indirect bandgap [16]. Practically, the most relevant parameters to measure are arguably the Hamaker constant, *H,* which quantifies the magnitude of vdW interactions between the two materials, and the Young's modulus, *E*, which describes the linear elastic response of the sample under strain [18]. The problem goes beyond the characterisation of 2D materials: the engineering of new polymeric materials and thin films, for example, also requires quantification of spatial variations in the *H* and E to correlate molecular changes in morphology with the resulting application performance [19, 20]. This is perhaps best illustrated by a technological example: polymeric multilayer thin films for coatings where their lifetime and toxicity depends on crystallisation processes due to dispersive forces [21]. Below a critical thickness of around 10 nm, vdW forces between the two adjacent polymeric layers become dominant over the stabilizing mechanical and capillary forces and they may thus amplify any interfacial instability eventually leading to the layer breakup [22]. The ability to quantify the cohesive dispersion forces and the material's mechanical properties *in situ* and with nanometric spatial resolution is therefore of paramount importance.

The simultaneous determination of both *H* and *E* while considering local defects is however challenging. Theoretical approaches such as DFT calculations tend to assume idealised defects or simply defect-free interfaces [16, 23]. Experimental approaches present also some limitations, in particular when determining *H*. *E* can be indeed studied by nanoindentation [24, 25] or atomic force microscopy (AFM) methods [25–27] with nanoscale spatial resolution. AFM, in particular, is an ideal candidate to directly compare topographical features with specific properties such as nanomechanical variations [28–31]. AFM enables mapping the topography of interfaces with sub-nanometer precision while simultaneously quantifying certain physical or chemical properties of the sample, thanks to its reliance on a nanoscale physical probe [32–36]. AFM operational modes are generally divided into static and dynamic, depending on whether the AFM cantilever is kept static at its base, or whether a periodic motion is imposed to it [37]. In most modern studies, the AFM is operated dynamically, with the probe externally vibrated to enhance sensing accuracy while better preserving the tip and the sample [28, 29, 33, 34, 37–39]. By tracking changes in the tip vibration frequency, amplitude and phase as it operates in close vicinity to a given sample, it is possible to reconstruct the local interaction force experienced by the tip near the sample's surface. For instance, dynamic AFM methods have been recently applied to soft and hard materials with their mechanical modulus and viscoelastic properties identified with great accuracy [27, 40]. In both static and dynamic modes, the contact between the tip and the sample can be described using the classical Hertz model for the case of a sphere in contact with an elastic half space [18, 27, 41]. The Hertz model is based on the assumptions of a frictionless and non-adhesive contact with the contact area significantly smaller than the radius of the sphere and with the deformation of both surfaces being perfectly reversible [18, 27]. Notably, the model assumptions may fall short in the plastic regime, or in the presence of non-negligible adhesive interactions between the AFM probe and the sample. In these cases, the Johnson–Kendall–Roberts (JKR) and the Derjaguin–Muller–Toporov (DMT) models offer a robust description of the interactions between the probe and a compliant or stiff substrate, respectively [18, 27].

Considering the determination of *H,* a wide range of experimental techniques have been applied from surface force apparatus [42] and immersion calorimetry [43] to optical techniques, such as dynamic light scattering [44] and ellipsometry [45]. These techniques however tend to be invasive [43] or average either over multiple locations or large areas [42–44, 46]. Also here, AFM has emerged as an ideal tool. For instance, using AFM static modes, the probe is moved laterally along the sample with vdW interactions reconstructed from friction-velocity curves and the activation energy necessary for the tip to start its motion over the substrate [47]. Static AFM modes offer the opportunity to reconstruct vdW interactions also studying the so-called jump-into-contact, that is, an instability in the cantilever motion due to the attractive force gradient being markedly greater than the cantilever spring constant [46]. Existing dynamic AFM however appear superior in comparison to static modes: they are minimally invasive and offer an excellent degree of control when studying single molecules adsorbed on a substrate [8, 9]. Still, existing AFM dynamic modes for the study of vdW interactions require specifically functionalised probes [8, 9, 48] and/or specialist equipment operating at ultrahigh vacuum and in some cases also at low

temperatures (5 K). This makes deriving local, nanoscale information often challenging.

To overcome these difficulties, we have developed a novel approach based on AFM where measurements can be conducted using standard commercial equipment operated in air or liquid. Here, we also address the problem of force reconstruction from AFM observables. Force reconstruction is challenging [39, 49, 50] because it usually relies on multiple deconvolution integrals to capture the multi-harmonic response of the vibrating cantilever to varying tip-sample interactions [51]. Several numerical methods have been developed [51] using slow time varying theory [49], iterative calculations [52] inversions of matrices [53], infinite summations of higher order derivatives [54], and Chebyshev polynomial expansions [55]. These approaches typically require heavy calculations and are often only valid for cantilever oscillation amplitudes significantly differing from the length scale of the interaction being probed [51]. The most popular method -the Sader and Jarvis method- provides a good approximation of the interaction forces while still using relatively simple integrals [39, 50, 51], but still requires the tip oscillation amplitude to be much smaller than the decay length of the interaction at play [51]. While not a problem in itself, this renders any direct quantification of H and E challenging, with most existing studies focusing on solvation effects (see e.g. reviews [56, 57]).

Here, using a development based on the viral equation, we derive an analytical expression that relates H and E to quantities directly observable in AFM measurements. This is rendered possible by combining the virial theorem with the DMT model (see e.g. [58] for a detailed review). The method can be easily implemented without the need of any specialized equipment and yields correct values using the standard dynamic operation conditions of commercial AFMs. The method is robust and can be used in both air and liquid, and with a wide range of oscillation amplitudes thus allowing for quantification across any desired length scale. For example, we use it to investigate the impact of nanoscale singularities and roughness on the derived quantities. We compare the results of the proposed method against literature values over a range of samples including some 2D and polymeric materials. We also run simulations verifying the experimental measurements. The proposed method offers a robust and non-invasive approach to accurately study mechanical properties and, above all, vdW interactions with high accuracy and spatial precision paving the way for efficiently designing of 2D heterostructures and new polymeric materials.

Results and discussion

The AFM is firstly operated in amplitude modulation (AM) to image the sample surface and highlight any nanoscale topographical defects or singularities (figure 1(a)). In this mode, the cantilever is driven with a constant oscillation amplitude and frequency with the changes in the former being used to re-construct the sample topography [33, 36, 37].

The nano-positioning system of the AFM allows selecting the nanoscale region of interest to probe by AFM force spectroscopy. Force spectroscopy is conducted in frequency modulation (FM) to allow straightforward separation of the dissipative and conservative forces experienced by the tip (figure 1(a)) [37]. In FM mode, the driving frequency is adjusted to always match the resonance frequency of the cantilever using a feedback loop that also ensures a 90° phase shift between the driving and tip oscillations. An additional feedback keeps the tip oscillation amplitude constant [37, 59].

Force spectroscopy measurements quantify the frequency shift, Δf, in the tip oscillation as it approaches the surface of the sample, yielding the characteristic frequency-distance (FD) curves where Δf is shown as a function of the tip-sample distance, d (figure 1). From FD curves, it is possible to extract the position a_0 of the transition from the attractive to repulsive region of the force experienced by the tip as it moves towards the surface.

The values of H and E are respectively deduced from the attractive ($d > a_0$) and repulsive ($d < a_0$) regions of the FD curve (figures 1(b)–(c)). The first step of the method is to derive an analytical expression for H and E based on the experimental parameters in conjunction with the DMT model. This is done using the virial theorem: for a full oscillation of the AFM cantilever vibrating at its first eigenfrequency, the virial of the tip-sample system, V_{tsc}, is equivalent to the time averaged kinetic energy of the tip [60]:

$$V_{tsc} = \frac{1}{T}\int_0^{T_0} F_{tsc}(d) \quad z(t)\mathrm{d}t, \tag{1}$$

where F_{tsc} is the conservative part of the interaction force between the cantilever tip ensemble and the surface of the sample, described by DMT force profile as [61]

$$F_{tsc} = \begin{cases} -\frac{HR}{6d^2} & d \geqslant a_0 \\ -\frac{HR}{6a_0^2} + \frac{4E\sqrt{R}}{3}(d)^{\frac{3}{2}} & d < a_0 \end{cases} \tag{2}$$

It is worth noting that this approach implicitly models dynamic sensing by means of a static indentation method (DMT). The conservative part of the interaction force when the cantilever taps the surface is effectively a form of contact resonance method (see figure 1(b)). The hard deformation of the tip/sample convoluted systems is however not taken into consideration, with the sample assumed to be significantly softer (smaller E) than the tip. Static indentation models have been widely used when reconstructing tip-sample interactions in dynamic AFM nanomechanical spectroscopy [25, 31, 40, 62]. The DMT model considers vdW forces and thus can effectively approximate both the attractive and repulsive regimes of nanoscale dynamic sensing [18, 63]. For the case of soft polymeric samples or where the attractive regime presents a shorter range in comparison to the deformation, the JKR model may be suggested as an option alternative to the DMT. Using the JKR, however, renders the method significantly more complex as the work of adhesion of the probe and the sample, and hence their surface free energies, should be also taken into account [18, 64]. Also, using the JKR model would require the reconstruction of

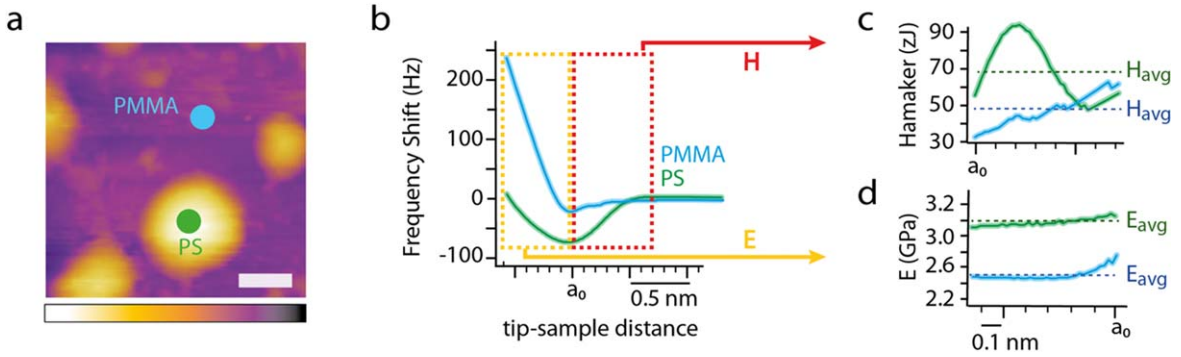

Figure 1. Effective Hamaker constant and Young's modulus derived from FM-AFM spectroscopy conducted at specific locations of a polymeric blend sample. The derivation procedure is illustrated for curves acquired over polymethylmethacrylate (PMMA) and polystyrene (PS) regions (a). As the tip approaches the sample surface, the oscillation frequency shifts due to tip-sample interactions (b). The minimum a_0 in the frequency shift marks the transition between regions dominated by attractive dispersion forces, H, (red rectangle in (b)) and repulsive elastic compression, E (yellow rectangle in (b)), respectively. Combining the associated frequency shift with the DMT model allows determination of the effective H (c) and E (d) from the relevant regions of the curve (see text for details). The average values of H and E over the relevant curve regions are shown as dashed lines in (c)–(d) and taken as the experimental values for the measured location. The colour and scale bars in the high-resolution amplitude modulation AFM image in (a) are 120 nm and 1 μm, respectively. Here, the measurements were conducted with silicon cantilevers coated with Ti/Ir (Asyelec.02, Oxford Instruments, London, UK); see below for the rationale behind the choice of these probes.

the tip-sample interaction forces [39, 50, 51]— a step the proposed method does not require as detailed below. Significantly, considering the caveats associated with modelling the indentation part of the curves and the large number of existing AFM-based approaches focusing precisely on determining the local Young's modulus [25, 31, 40, 62], the present study places the emphasis on the non-contact region of the oscillation and the quantification of dispersive forces.

In FM-AFM, the instantaneous displacement $z(t)$ of the cantilever oscillating with amplitude, A, is given by

$$z(t) = A\cos\left(\omega t + \frac{\pi}{2}\right) \tag{3}$$

Thus, the interaction potential in equation (1) can be approximated as [37, 60]

$$V_{tsc} = -A^2 k\frac{\Delta f}{f_0} \tag{4}$$

where k is the cantilever flexural spring constant and f_0 the resonance frequency of the cantilever far from the sample.

Combining equations (1), (2) and (4) leads to the following analytical expressions for H and E, the effective Hamaker constant and Young's modulus of the combined tip-sample system, (see supplementary material section 1 for a detailed derivation of the expressions):

$$H = \frac{6kA^3\Delta \mathrm{f}}{Rf_0}\left[\left(\frac{d+A}{A}\right)^2 - 1\right]^{3/2} \qquad d \geqslant a_0 \tag{5}$$

$$E = \frac{k\Delta f}{f_0\sqrt{R}}\left[\frac{\sqrt{8A^3}}{(a_0-d)^2} + \frac{1}{\sqrt{(a_0-d)}}\right] + \frac{H\sqrt{R}}{8a_0^2(a_0-\mathrm{d})^{3/2}} \qquad d < a_0 \tag{6}$$

We note that while H is defined for a specific pair of interacting materials, E describes an intrinsic property of a given material. Here, E comprises information from both the sample and the indenter through the well-known relationship [18, 65]:

$$E = \left(\frac{1-\nu_m^2}{E_m} + \frac{1-\nu_t^2}{E_t}\right)^{-1}, \tag{7}$$

where $\nu_m(\nu_t)$ and E_m (E_t) are the Poisson's ratio and Young's modulus of the material (the indenting tip).

As shown in figure 1(b), (E) is reconstructed for the FD regime where the cantilever tip is indenting into the material, thus ensuring full contact between the two. The oscillation amplitude being constant provides a key advantage for FM-AFM spectroscopy allowing directly measuring the indentation length as the cantilever moves towards the surface [31, 66, 67].

Practically, at least, 100 FD curves are acquired per location and subsequently averaged; then, using the average FD curve, the experimentally determined values of H and E for the location considered are taken as the average values over the attractive, and repulsive regime, respectively, and their uncertainty taken as the standard error. This averaging procedure accounts for the uncertainty related to the imposed DMT force profile and measurement noise.

One key point to highlight is that the derived Hamaker constant does not represent single atomistic interactions but rather an average over a small (typically $<$100) number of molecules or atoms. Existing theoretical and experimental methods based on an atomistic description allow investigating vdW dispersion coefficients [8] and non-additive screening [4] between single atoms, as well as molecular adsorption distances [9], but measurements typically need to be conducted with specialist equipment in ultra-high vacuum [8, 9]. Here, H is reconstructed using a simple continuum, nanoscale model thus inherently assuming average properties over the surface area probed by the AFM tip apex. The use of a continuum assumption is also responsible for the variation of H with distance observed in figure 1(c). This is mitigated by averaging over short distances and we hence refer to H as an

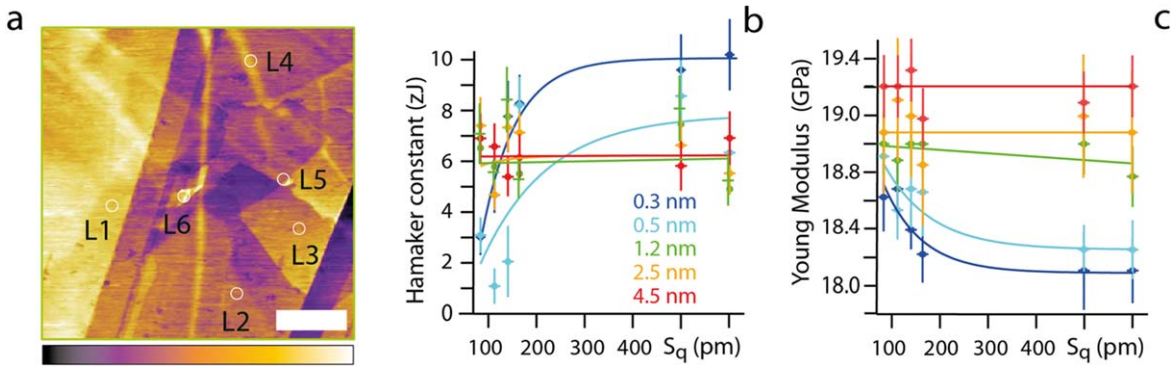

Figure 2. Impact of nanoscale features on the effective Hamaker constant and Young's modulus at the HOPG-water interface. Imaging of the water-HOPG interface shows a wide variety of features such as step edges, terraces, point-like defects (a). Representative features with increasing local roughness (L1 → L6) are probed using FM spectroscopy. Each location is investigated with five different oscillation amplitudes (0.3, 0.5, 1.2, 2.5 and 4.5 nm). At small oscillation amplitudes (<1 nm), H and E vary with the sample roughness (b)–(c). This is no longer the case for larger amplitude where H and E appear roughness independent due to the local features being averaged in the measurements. The surface roughness is the root mean square value (S_q) [18] averaged over an area of ∼ 50 nm^2 to account for possible experimental drift [26]. The nonlinear evolution of H and E as functions of S_q has been fitted with an exponential which converges to an average value for oscillations >0.5 nm. The colour and scale bars in the high-resolution amplitude modulation AFM image in (a) are 2 nm and 400 nm, respectively. Here, the measurements were performed with Arrow UHF silicon cantilevers (Nanoworld, Switzerland); see the main text for the rationale.

effective Hamaker constant. Further improvements to the model could include quantum many-body treatment for the non-additive nature of vdW interactions [15], but such a treatment goes beyond the scope of this paper. Here, the focus is instead placed on developing an approach which can be rapidly and simply implemented with commercial AFMs, and applied both in air and liquid. A further advantage of the proposed method over existing approaches is the fact that it bypasses the need for any fitting procedures [68, 69] inherent to force reconstruction strategies, significantly reducing the error on the analysis. Additionally, the direct relationship between Δf, H and E makes the analysis considerably simpler and faster. Figure 1 further highlights the potential of the proposed method in investigating local differences in H and E forces over a polymer blend sample. As expected, distinct polymethylmethacrylate (PMMA) and polystyrene (PS) domains are visible. In both cases, the effective Young's modulus decreases as the tip further indents into the material due to an increase in adhesion between the cantilever and the sample, a phenomenon well documented [18]. The behaviour of H, however, shows significant differences between PMMA and PS likely due to their different hydrophilicity and the measurements being conducted in ambient conditions ($T = 25$ °C, relative humidity, RH = 40 ± 5%). PMMA and PS exhibit water contact angles of 67° [70] and 86° [71], respectively, creating a thin water film on PMMA that changes the dielectric constant of the intervening medium. H values derived over the attractive region can vary also due to the imposed DMT force profile and measurement noise. This is mitigated by taking the average value over the entire region. To validate the technique, we used a numerical approach with computer simulations based on a fourth-order Runge–Kutta algorithm [72, 73], and exploring materials with H ranging from ∼10^{-21} up to 10^{-19} J and E from ∼0.1 GPa to >4 GPa. The interest of this approach is the ability to test a wider range of materials properties without changing other parameters such as surface chemistry. The simulation results show the robustness of the method in quantifying H and E for all the samples (figures S1–2 and supplementary material section 2).

Before conducting a similar experimental validation on different samples, it is necessary to ascertain the robustness of the method in terms of experimental parameters. Since H and E are only observable over specific regions of the FD curves, it is likely that the choice of tip oscillation amplitude will impact the measurements. This is practically important when conducting AFM measurement because the choice of amplitude affects the size of the features that can be resolved, but also the signal-to-noise of the measurement. We investigate this issue systematically on a highly orientated pyrolytic graphite (HOPG) sample immersed in pure water. The water-HOPG interface is crucial to a wide range of technological systems from vdW-based interfacial self-assembly [74] and catalysis [75] to surfactants and lubrication [28], and is hence used here as a test system. HOPG surfaces present a range of structural features from step edges to asperities [28], offering an ideal platform to test the ability of our method with different operating amplitudes. We first image the water-HOPG interface (figure 2(a)), revealing various surface features such as step edges, terraces, point-like defects and other singularities. Choosing 6 different locations with increasing local roughness (labelled as L1–6, figure 2(a)) we conduct spectroscopic measurements with a range of oscillation amplitudes and derive H and E in each case. Roughness is arguably the simplest metric to characterise the local topography of a nanoscale region or surface sites [18, 28]. The reconstructed average values for H and E are presented as functions of roughness (figures 2(b)–(c)). At small amplitudes (0.3–0.5 nm), a clear evolution is visible with regions exhibiting smaller roughness showing, overall, smaller H and greater E (figures 2(b)–(c)). This trend vanishes at larger amplitudes where H and E appear to converge to average

values independently of the roughness. The fact that smaller oscillations amplitudes are more sensitive to local variations in nanoscale features is expected [28, 33]. The present measurements show that, for measurements of H and E, this effect tends to occur when the oscillation amplitude is comparable or smaller than the size of the local features. In such cases, H increases due to the larger effective surface areas interacting with the measuring tip, when compared to a perfectly flat region [18]. In contrast, the apparent E decreases due to sample become more deformable locally at asperities and defects [18]. Using oscillation amplitudes larger than the features length scale results in averaging out any singularities and probing an effectively *homogeneous* sample surface. H and E then tend to converge to average values which are in relatively good agreement with theoretical expectations and experimental results from the literature (2–30 zJ and 18–24 GPa, respectively). This is an important results because it demonstrates that the method is capable of distinguishing the contributions of local nanoscale features, something usually neglected by existing measurement techniques and models [76–88]. Previous dynamic and contact mode AFM studies have highlighted the fact that H values tend to be affected by roughness and nanoscale features [89, 90]. This was achieved by implementing an AFM system within a transmission electron microscope (TEM), with the measurements performed in vacuum. While highly accurate, the need for a combined AFM-TEM system significantly limits its broad applicability [89]. Here, the proposed method can be easily implemented into standard commercial AFMs for measurements at ambient conditions and on any materials.

It is furthermore worth mentioning that the choice of oscillation amplitude has a crucial importance when using numerical methods in force reconstruction. The numerical deconvolution of the force can be ill-posed resulting in erroneous forces values, extremely sensitive to arbitrarily small errors in the oscillation amplitude. A solution to this ill-posed problem is to adjust the oscillation amplitude by means of an inflection point test [91]. The inflection point test is based on evaluating the first and third derivatives of the force at each inflection point to verify whether the curvature of the reconstructed force may change too rapidly with a consequent loss in information. Experimentally, the determination of inflection points and the calculation of the first and third derivatives are far from trivial due to the discrete nature of the data and noise with the need of data filtering based on an arbitrary choice of parameters. Experimental studies furthermore suggest that the test may yield results for the oscillation amplitude which do not maximize the signal-to-noise ratio [92]. Our proposed method offers an analytical equation that avoids the ill-posed problem in force deconvolution, allowing for a wide range of oscillation amplitudes to be used.

Using roughness independent (>3 nm) amplitudes, we then comparatively test the proposed method over 8 different samples representative of 2D materials and polymers in air at ambient conditions (see Methods section below): muscovite mica, HOPG, molybdenum disulfide (MoS_2), grown monolayers of WSe_2, $MoTe_2$ and hexagonal boron nitride (h-BN) and unmodified unstained microphase separated polystyrene-b-polymethylmethacrylate (PS-PMMA). The first three samples (HOPG, mica and MoS_2) act as a reference: the Hamaker constants describing their interaction with silicon (the AFM tip material) have previously been experimentally determined. WSe_2, $MoTe_2$ and h-BN are selected as representative 2D-materials for which, to the best of our knowledge, only theoretical predictions for H are available. Finally, a microphase separated PS-PMMA mixture is used as representative of polymeric materials. These polymers also offer a benchmark to assess the spatial accuracy of the method, allowing the selective probing of PS or PMMA domains (see figure 1(a)). The representative 2D materials are tested with commonly used silicon cantilevers [29, 47, 93], whereas the experiments on PS-PMMA are performed with Ti/Ir coated cantilevers. The use of different combination of AFM probes and substrates is deliberate, to validate the general applicability of the proposed method independently from a specific system or operating conditions. Additionally, the choice of tip materials used in this study is motivated by the relevance of silicon-based substrates for the growth of 2D materials, and the routine use of Ti nanofibers and Ir complexes with PS and PMMA polymers in photovoltaics [94], pH electrodes for harsh environmental conditions [95] and medical devices [96].

The Young's moduli of all the samples have been previously established with various experimental techniques [76–78, 84, 85, 88, 97, 98], offering a straightforward assessment of equation (5). In all cases, the sample modulus E_m is derived, using equation (7) and assuming a tip modulus of $E_t \sim 500$ GPa for Ir [99] and $E_t \sim 150$ GPa for Si [100], and Poisson ratios of 0.26 (Ir) and 0.23 (Si) [65, 100–106]. The Poisson ratios for the materials are taken from 65, 79, 107–112. The results are shown in figure 3 for all the materials studied.

Comparison between the derived and literature values indicate an excellent agreement within error, except for $MoTe_2$ and WSe_2 where larger differences are visible. Even for these materials, the differences between measured and literature values are $\sim 30\%$ within error, a remarkable feat considering the broad range of moduli being probed. The specific experimental conditions and sample preparation are also likely to influence the values measured with no means of ensuring identical conditions between the present and literature values. The good agreement of our measured values with the literature for the PS-PMMA polymeric blend rules out tip convolutions effects [28, 115]: after selecting the region of interest (figure 1), our approach accurately investigates its nanomechanical properties without any evident tip geometry dependent artifacts or bias due to the cantilever inclination with respect to the sample surface [115]. Further studies are however needed to validate the impact of probe geometry on the proposed method and to further implement it also using available models for AFM tips/surface interactions accounting for the tip geometry [2, 66, 116]. Additionally, although the Young moduli derived for the stiffer material appear in good agreement with the literature, the measurement is ambiguous since the tip itself has comparable stiffness. A more sophisticated model considering the tip deformation may be needed in some cases.

Overall, figure 3 validates the approach developed in this study to determine E, a well-characterized quantity. Determining

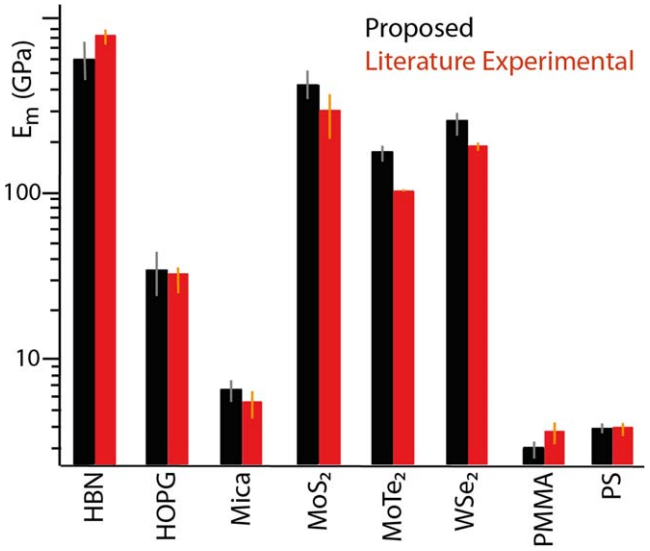

Figure 3. Comparison of the E_m values derived in this study using a combination of FM-AFM spectroscopy and equations (5) and (7) (black) with published values from other experimental studies (red). The measured and literature value agree within error for all the materials except for $MoTe_2$ and WSe_2 where the values differ by ~30% within error. The literature values are from the following refs: HBN [77], HOPG [76, 78], mica [97], MoS_2 [84, 113, 114], $MoTe_2$ [84, 98], WSe_2 [85, 88], PMMA [86] and PS [86]. Note the log scale to aid comparison across the wide range of values.

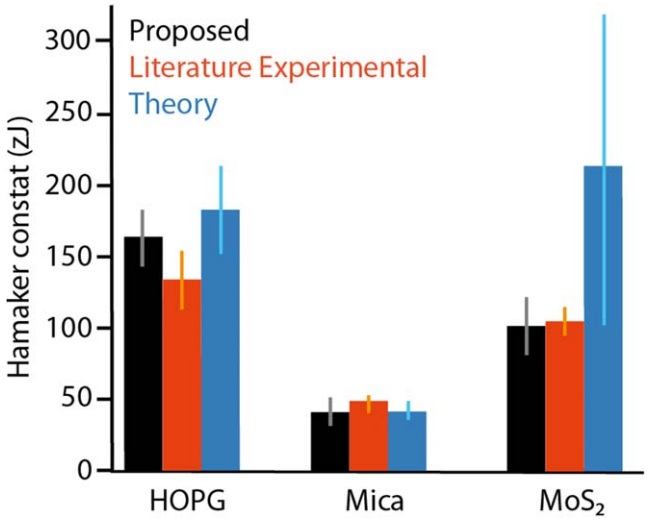

Figure 4. Comparison of H constants measured in this study (black) with experimental values from the literature (red) [47, 121] and theoretical predictions (blue). The literature experimental values are from [121] for mica, and [47] for HOPG and MoS_2. In all cases, the H values represent the interactions between the stated material and the silicon AFM tip in air at ambient conditions; the different intervening medium in comparison to the measurements shown in figure 2 (water) accounts for the different values of H for HOPG. For mica, the literature value was obtained by linear interpolation of the reported dry and water-saturated values to match our 40% experimental humidity. The theoretical predictions assume a homogeneous ice-like layer of adsorbed water molecules on the surface, and the silicon cantilever undergoing an effective surface oxidation (see supplementary material section 3). Measurements over mica could not be achieved in water, presumably due to its strong hydrophilicity [18, 29, 33]. The error bars on the theoretical predictions represent the range of refractive indices and dielectric constants reported in the literature (see supplementary material section 3).

H is more challenging with limited experimental benchmarking available. For five out of the eight materials investigated here, only theoretical predictions are available, based on the Lifshitz theory [117–119]. The theoretical calculations assume that the tip, the sample and the medium in-between are all perfectly homogeneous. This is obviously a simplification, especially for the in-between medium where condensation water molecules and adsorbed contaminants can affect the dielectric constant [120]. We therefore first validate the proposed method with the three systems for which experimental H values are available: HOPG, mica, and MoS_2, each interacting with commercial silicon or silicon nitride tips [47, 121]. Silicon tips are well-known to form a surface oxide layer when exposed to ambient conditions, something common for all commercial tips. It is therefore reasonable to assume the silicon tips to behave as silicon nitride since the latter exhibits properties in-between pure silicon and silicon oxide (see supplementary material section 3 for the relevant data). Our experiments being conducted in ambient conditions, water molecules tend to adsorb at the surface of the sample and the tip forming complete ordered layers at hydrophilic interfaces. On mica, ambient humidity creates ice-like structure due to epitaxial effects with the substrate lattice constant approximately matching that of the hexagonal ice basal plane [33]. To some extent, ice-like layer can also be assumed to form at the interface with HOPG and MoS_2 which lie at the boundary between hydrophilic and hydrophobic (see supplementary material section 4). In principle, adsorption of airborne hydrocarbons can also affect the measurements and is well known to increase hydrophobicity over time [122], but the present measurements were conducted on freshly cleaved surfaces. In all cases, the tip is bound to have an absorbed water layer on its surface and we hence always derived theoretical prediction assuming an ice-like water layer between the tip and the different substrates [29] (see supplementary material section 3 for the details on the theoretical calculations). Figure 4 shows, for the three materials, the comparison of measured H versus the experimental data obtained from the literature and theoretical predictions. For each material the measured, literature and theoretical data agree within error, with a particularly good agreement between the measured and the literature values. In the case of mica, the literature values were adjusted to match our experimental humidity (40% ± 5%) by interpolating the values reported for a dry [117, 121] and humidity saturated environment [117]. In the case of MoS_2, the theoretical prediction appears way off, despite agreeing with the experimental values when the large error is considered. Relaxing the assumption of a water layer would only increase the predicted H value, suggesting a fundamental problem with the prediction. Part of the issue comes from the difficulty in obtaining a relevant refractive index for MoS_2, a key parameter in the prediction. Depending on the publications and the range of wavelengths considered [123–125], reported refractive index values can vary by more than 100% rendering objective predictions challenging.

Aside from the difficulty with the theoretical prediction for MoS_2, the excellent agreement between the measured, reported

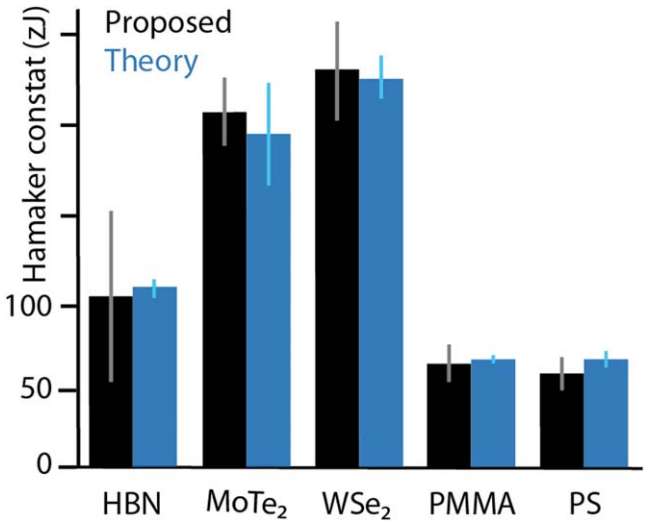

Figure 5. Comparison of the values for H derived experimentally with the proposed method and calculated from theory. As for the previous materials, the theoretical calculations assume an adsorbed layer of water molecules on the surfaces (ambient conditions) thereby affecting the dielectric response of the intervening medium [130, 131] (see also supplementary material section 3).

and theoretical H values validates the proposed method. We therefore derived the first experimental H constants for the other five materials with only theoretical calculations as a point of comparison. All the materials probed are weakly hydrophilic (see supplementary material section 4) and an epitaxial water layer is expected (also assumed in the calculations). This is a common feature for some of the most wide spread 2D materials based on graphene and transition metal dichalcogenides [126], as well as for a wide range of technologically relevant polymers with applications, for example, in drug delivery [127], wastewater treatment [128] and thermally insulating foams [129]. The calculations were therefore conducted under the same assumptions as before. The results, presented in figure 5, show an excellent agreement between our measurements and the theoretical predictions within error.

Taken together our experimental results validate the proposed experimental method and show that it is possible to derive simultaneously H and E with high spatial accuracy and without damaging either the probe or the sample.

It is worth mentioning that the proposed method approximates the probe surface interacting with the substrate as the tip apex. While our simplified modelling is among the most popular approaches in the AFM community [18, 31, 46, 60, 132, 133], it may be argued that, vdW attractions being relatively long-ranged, the tip shank contribution should be considered. Models have been hence developed in this sense [68, 134]. These approaches are however highly sensitive to the choice of fitting parameters [134]. Furthermore, in the case of vdW attractive forces range being smaller than the tip radius, these methods may overestimate the Hamaker constant. This may explain why, incorporating the tip shank contribution in our model, the results differ from the theoretical or literature values (figure S3 in the supplementary material section 5). It should be also noted that this additional contribution is only approximated (see equation S18 in supplementary material section 5) and has not been analytically resolved within our proposed method.

It is also worth discussing some limitations and possible sources of error in conducting the measurements. First, as obvious from the previous discussion, environmental factors such as humidity and airborne contamination of the material and the tip can dramatically influence the value derived for H. The issue is not specific to the proposed method but common to all experimental measurements of dispersion forces. Measurements should therefore be conducted in an environment which best replicates that of the desired application, and with a suitable degree of care. Second, the methodology itself relies on the accurate determination of the probe's stiffness [135, 136], its effective tip radius of curvature [137], the pull-off deflection force and the cut-off distance [121]. These parameters being fundamental when reconstructing physical quantities from standard AFM spectroscopy measurements, there exist, however, well established protocols [2, 37, 138] to precisely and accurately determine them minimising the associated uncertainty. It is therefore possible to accurately and reliably quantify the error on H and E resulting from measurements with the proposed method.

Conclusions

In this study, we present a fully analytical method to derive the Hamaker constant and Young's modulus of a sample material from experimental observables acquired in AFM spectroscopic measurements. The derived Hamaker constant and Young's modulus represent an average over a small (typically <100) number of molecules or atoms. The method offers a spatial resolution comparable to the size of the AFM tip (typically <10 nm) and can be easily implemented on most commercial AFMs. We validate our approach on a range of materials, from relatively stiff 2D materials to compliant polymers films, paving the way for its adoption in the nanoscale design of 2D materials and polymer-based devices. It could, for example, help disentangle the effect of doping on functional coatings [139, 140] and energy storage materials [141]. The ease of use and the high spatial resolution would also help provide new insights into the role of vdW forces in the function and assembly of 2D heterostructures on different substrates [6, 142].

Methods

Materials

Experiments are conducted using a commercial Cypher ES AFM (Oxford Instruments, CA, USA) equipped with temperature control. We use two types of commercial cantilevers with their flexural calibration being performed using their thermal spectrum [143]:

1. Arrow UHF silicon cantilevers (Nanoworld, Switzerland). Arrow cantilevers were found to have a stiffness k_f in the range 1.6–5.0 N m^{-1}, a Q-factor of 360 $\pm$ 10 and a

flexural resonance frequency of 2040 ± 50 kHz. The mechanical properties of the cantilevers are consistent with the literature [29, 144].

2. Asyelec.02 silicon cantilevers coated with Ti/Ir (5/20) (Oxford Instruments, London, UK). The probes are found to have flexural stiffness, *k,* of 46.0 ± 0.3 nN nm^{-1}, a Q-factor of 630.0 ± 0.3 and a resonance frequency of 318 ± 1 kHz. In comparison to standard silicon tips [29, 145], the stiffness and the Ir-coating of tips ensures increased sensitivity through higher Q-factor [37] and high wear resistance [146], respectively.

High-quality V1 muscovite mica discs, HOPG and MoS_2 were purchased from SPI supplies, West Chester, PA, USA; grown monolayers of WSe_2, $MoTe_2$ and h-BN, each of them transferred to a SiO_2/Si substrate, were custom made by 2D Semiconductors, NY, USA; unmodified unstained microphase separated PS-PMMA was purchased from Nanosurf AG, Liestal, Switzerland. Thorough cleaning procedures were implemented as detailed in the supplementary material section 6.

Imaging

All the experiments are performed in air at 25 °C, unless otherwise specified (e.g. HOPG fully immersed in water, figure 2). All the experiments were performed ensuring that at the time of the measurements the ambient RH was within the range 40% ± 5%, thus minimizing any variations in the potential capillary forces experienced by the probe. The RH was monitored with a thermo-hygrometer (Fluka Corporation, Washington, USA). Thermal equilibrium is achieved ensuring that the cooling/heating rate of the temperature control system within the AFM is constant for, at least, 20 min [29, 138]. The sample surfaces are imaged both before and after performing force spectroscopy. This allows selecting, with sub-nanometer precision, the locations to probe by force spectroscopy, as well as ensuring the absence of any significant drift after conducting the spectroscopy. Furthermore, this also helps rule out the presence of any adsorbed contaminants directly visible when imaging. High-resolution imaging is performed in amplitude modulation AFM (AM-AFM). In this mode, the cantilever is oscillated at a frequency close to resonance. Away from the material surface, the cantilever oscillates with a free amplitude A_0. As the tip approaches the sample, the oscillation amplitude is reduced due to the interactions with the sample surface. The material surface is raster-scanned keeping a set point amplitude, A_s, constant by means of a feedback loop. The ratio A_s/A_0 is set as high as possible so as to ensure gentle imaging. The sample topography is reconstructed using the amplitude corrections. The phase lag between the cantilever oscillation and the driving oscillation can vary freely and provides information on the tip-sample interactions [28, 29, 147].

Force spectroscopy is performed in frequency modulation. The cantilever approaching the sample surface, its oscillation amplitude and frequency are kept constant using two feedback loops. For the measurements exploring the role of oscillation amplitude presented in figure 2, the HOPG-water is investigated using an Arrow UHF cantilever with 5 different amplitudes (0.3, 0.5, 1.2, 2.5, 4.5 nm). The set amplitude is 3.00 nm for the 2D-materials and 8.00 nm for the PS-PMMA (figures 3–5). Frequency and amplitude corrections are acquired as a function of the tip-sample distance [37] over >3 (typically 5) different locations for each substrate resulting in >100 force-distance curves that are subsequently averaged. Each set of experiments, including both imaging and spectroscopy, is repeated at least three times to ensure reproducibility.

Data availability statement

All data that support the findings of this study are included within the article (and any supplementary files).

Competing interests

The Authors declare no Competing Financial or Non-Financial Interests.

Author contributions

A. F. P. conceived the original idea and developed the mathematical model. C. C. conceived, planned and conducted all the experiments. C.C. and A. F . P. analysed the data. All the others contributed to writing the paper. C. C. is grateful to the Institute of Advanced Studies, Durham University and to the Physics Department, Durham University (Developing Talent Scheme) for the financial support. K. V. acknowledges funding from EPSRC (EP/ S028234/1).

ORCID iDs

Clodomiro Cafolla https://orcid.org/0000-0002-8759-8775
Kislon Voïtchovsky https://orcid.org/0000-0001-7760-4732
Amir Farokh Payam https://orcid.org/0000-0002-6433-2261

References

[1] Novoselov K S, Mishchenko A, Carvalho A and Castro Neto A H 2016 2D materials and van der Waals heterostructures *Science* **353** aac9439
[2] Garcia R 2020 Nanomechanical mapping of soft materials with the atomic force microscope: methods, theory and applications *Chem. Soc. Rev.* **49** 5850–84
[3] Labardi M and Capaccioli S 2021 Tuning-fork-based piezoresponse force microscopy *Nanotechnol.* **32** 445701
[4] Tsoi S, Dev P, Friedman A L, Stine R, Robinson J T, Reinecke T L and Sheehan P E 2014 van der Waals

screening by single-layer graphene and molybdenum disulfide *ACS Nano* **8** 12410–7
[5] Gobre V V and Tkatchenko A 2013 Scaling laws for van der Waals interactions in nanostructured materials *Nat. Commun.* **4** 2341
[6] Li Z *et al* 2020 Efficient strain modulation of 2D materials via polymer encapsulation *Nat. Commun.* **11** 1151
[7] Rokni H and Lu W 2020 Direct measurements of interfacial adhesion in 2D materials and van der Waals heterostructures in ambient air *Nat. Commun.* **11** 5607
[8] Wagner C, Fournier N, Ruiz V G, Li C, Müllen K, Rohlfing M, Tkatchenko A, Temirov R and Tautz F S 2014 Non-additivity of molecule-surface van der Waals potentials from force measurements *Nat. Commun.* **5** 5568
[9] Schuler B, Liu W, Tkatchenko A, Moll N, Meyer G, Mistry A, Fox D and Gross L 2013 Adsorption geometry determination of single molecules by atomic force microscopy *Phys. Rev. Lett.* **111** 106103
[10] Wang Y *et al* 2020 Robust ferromagnetism in highly strained $SrCoO_3$ thin films *Phys. Rev.*V **10** 021030
[11] Li W *et al* 2020 Atomic-scale control of electronic structure and ferromagnetic insulating state in perovskite oxide superlattices by long-range tuning of BO6 octahedra. *Adv. Funct. Mater.* **30** 2001984
[12] Glavin N R, Rao R, Varshney V, Bianco E, Apte A, Roy A, Ringe E and Ajayanet P M 2020 Emerging applications of elemental 2D materials *Adv. Mater.* **32** 1904302
[13] Zhang S, Ma T, Erdemir A and Li Q 2019 Tribology of two-dimensional materials: from mechanisms to modulating strategies *Mater. Today* **26** 67–86
[14] Ambrosetti A, Ferri N, DiStasio R A and Tkatchenko A 2016 Wavelike charge density fluctuations and van der Waals interactions at the nanoscale *Science* **351** 1171–6
[15] Hauseux P, Nguyen T T, Ambrosetti A, Ruiz K S, Bordas S P and Tkatchenko A 2020 From quantum to continuum mechanics in the delamination of atomically-thin layers from substrates *Nat. Commun.* **11** 1651
[16] Tripathi M *et al* 2021 Structural defects modulate electronic and nanomechanical properties of 2D materials *ACS Nano* **15** 2520–31
[17] Guo H W, Hu Z, Liu Z B and Tian J G 2021 Stacking of 2D materials *Adv. Funct. Mater.* **31** 2007810
[18] Mate C M and Carpick R W 2019 *Tribology on the Small Scale: a Modern Textbook on Friction, Lubrication, and Wear* (Oxford University Press)
[19] Vashisth A, Khatri S, Hahn S H, Zhang W, van Duin A C T and Naraghi M 2019 Mechanical size effects of amorphous polymer-derived ceramics at the nanoscale: experiments and ReaxFF simulations *Nanoscale* **11** 7447–56
[20] Li Q, Barrett D G, Messersmith P B and Holten-Andersen N 2016 Controlling hydrogel mechanics via bio-inspired polymer-nanoparticle bond dynamics *ACS Nano* **10** 1317–24
[21] Vanroy B, Wü M and Napolitano S 2020 Remotely controlling the crystallization of thin polymer coatings *Macromolecules* **53** 4882–8
[22] Kadri K, Peixinho J, Salez T, Miquelard-Garnier G and Sollogoub C 2021 Dewetting of a thin polymer film under shear *Polymer* **235** 124283
[23] Schulman D S, Arnold A J and Das S 2018 Contact engineering for 2D materials and devices *Chem. Soc. Rev.* **47** 3037–58
[24] Oliver W C and Pharr G M 2004 Measurement of hardness and elastic modulus by instrumented indentation: advances in understanding and refinements to methodology *J. Mater. Res.* **19** 3–20
[25] Liu Y, Sokolov I, Dokukin M E, Xiong Y and An Peng P 2020 Can AFM be used to measure absolute values of Young's modulus of nanocomposite materials down to the nanoscale? *Nanoscale* **12** 12432–43
[26] Rejhon M, Lavini F, Khosravi A, Shestopalov M, Kunc J, Tosatti E and Riedo E 2022 Relation between interfacial shear and friction force in 2D materials *Nat. Nanotechnol.* **17** 1280–7
[27] Cellini F, Gao Y and Riedo E 2019 Å-Indentation for non-destructive elastic moduli measurements of supported ultra-hard ultra-thin films and nanostructures *Sci. Rep.* **9** 4075
[28] Cafolla C, Foster W and Voïtchovsky K 2020 Lubricated friction around nanodefects *Sci. Adv.* **6** eaaz3673
[29] Cafolla C and Voïtchovsky K 2020 Impact of water on the lubricating properties of hexadecane at the nanoscale *Nanoscale* **12** 14504–13
[30] Mangolini F, McClimon J B, Rose F and Carpick R W 2014 Accounting for nanometer-thick adventitious carbon contamination in x-ray absorption spectra of carbon-based materials *Anal. Chem.* **86** 12258–65
[31] Payam A F, Morelli A and Lemoine P 2021 Multiparametric analytical quantification of materials at nanoscale in tapping force microscopy *Appl. Surf. Sci.* **536** 147698
[32] Melcher J, Martínez-Martín D, Jaafar M, Gómez-Herrero J and Raman A 2013 High-resolution dynamic atomic force microscopy in liquids with different feedback architectures *Beilstein J. Nanotechnol.* **4** 153–63
[33] Cafolla C and Voïtchovsky K 2018 Lubricating properties of single metal ions at interfaces *Nanoscale* **10** 11831–40
[34] Ricci M, Trewby W, Cafolla C and Voïtchovsky K 2017 Direct observation of the dynamics of single metal ions at the interface with solids in aqueous solutions *Sci. Rep.* **7** 43234
[35] Ricci M, Spijker P and Voïtchovsky K 2014 Water-induced correlation between single ions imaged at the solid–liquid interface *Nat. Commun.* **5** 4400
[36] Miller E J, Trewby J, Payam A F, Piantanida L, Cafolla C and Voitchovsky K 2016 Sub-nanometer resolution imaging with amplitude-modulation atomic force microscopy in liquid *J. Vis. Exp.* **118** e54924
[37] García R and Pérez R 2002 Dynamic atomic force microscopy methods *Surf. Sci. Rep.* **47** 197–301
[38] Payam A F, Ramos J R and Garcia R 2012 Molecular and nanoscale compositional contrast of soft matter in liquid: Interplay between elastic and dissipative interactions *ACS Nano* **6** 4663–70
[39] Sader J E, Uchihashi T, Higgins M J, Farrell A, Nakayama Y and Jarvis P 2005 Quantitative force measurements using frequency modulation atomic force microscopy- theoretical foundations *Nanotechnology* **16** S94
[40] Herruzo E T, Perrino A P and Garcia R 2014 Fast nanomechanical spectroscopy of soft matter *Nat. Commun.* **5** 3126
[41] Labuda A, Kocun M, Meinhold W, Walters D and Proksch R 2016 Generalized Hertz model for bimodal nanomechanical mapping *Beilstein J. Nanotechnol.* **7** 970–82
[42] Horn R G, Clarke D R and Clarkson M T 1988 Direct measurement of surface forces between sapphire crystals in aqueous solutions *J. Mater. Res.* **3** 413–6
[43] Médout-Marère V 2000 A simple experimental way of measuring the Hamaker constant A_{11} of divided solids by immersion calorimetry in apolar liquids *J. Colloid Interface Sci.* **228** 434–7
[44] Zhang Y, Tian R, Yang S, Guo X and Li H 2021 Toward an approach for determining the Hamaker constant of soft materials using dynamic light scattering *Colloids Surf.*A **630** 127604
[45] Shahidzadeh N, Bonn D, Ragil K, Broseta D and Meunier J 1998 Sequence of two wetting transitions induced by tuning the hamaker constant *Phys. Rev. Lett.* **80** 3992–5
[46] Das S, Sreeram P A and Raychaudhuri A K 2007 A method to quantitatively evaluate the Hamaker constant using the

jump-into-contact effect in atomic force microscopy *Nanotechnology* **18** 035501
[47] Krajina B A, Kocherlakota L S and Overney R M 2014 Direct determination of the local Hamaker constant of inorganic surfaces based on scanning force microscopy *J. Chem. Phys.* **141** 164707
[48] Polesel-Maris J, Guo H, Zambelli T and Gauthier S 2006 Mapping van der Waals forces with frequency modulation dynamic force microscopy *Nanotechnology* **17** 4204
[49] Payam A F, Martin-Jimenez D and Garcia R 2015 Force reconstruction from tapping mode force microscopy experiments *Nanotechnology* **26** 185706
[50] Sader J E and Jarvis S P 2004 Accurate formulas for interaction force and energy in frequency modulation force spectroscopy *Appl. Phys. Lett.* **84** 1801–3
[51] Kim S, Ko J-H and Jhe W 2021 Universal theory of dynamic force microscopy for exact and robust force reconstruction using multiharmonic signal analysis *Phys. Rev. Lett.* **126** 076804
[52] Gotsmann B, Anczykowski B, Seidel C and Fuchs H 1999 Determination of tip-sample interaction forces from measured dynamic force spectroscopy curves *Appl. Surf. Sci.* **140** 314–9
[53] Giessibl F J 2001 A direct method to calculate tip-sample forces from frequency shifts in frequency-modulation atomic force microscopy *Appl. Phys. Lett.* **78** 123–5
[54] Lee M and Jhe W 2006 General theory of amplitude-modulation atomic force microscopy *Phys. Rev. Lett.* **97** 036104
[55] Hu S and Raman A 2008 Inverting amplitude and phase to reconstruct tip-sample interaction forces in tapping mode atomic force microscopy *Nanotechnology* **19** 375704
[56] O'Shea S J, Gosvami N N, Lim L T W and Hofbauer W 2010 Liquid atomic force microscopy: solvation forces, molecular order, and squeeze-out *Jpn. J. Appl. Phys.* **49** 08LA01
[57] Ludwig M and von Klitzing R 2020 Recent progress in measurements of oscillatory forces and liquid properties under confinement *Curr. Opin. Colloid Interface Sci.* **47** 137–52
[58] Butt H J, Cappella B and Kappl M 2005 Force measurements with the atomic force microscope: technique, interpretation and applications *Surf. Sci. Rep.* **59** 1–152
[59] Payam A F 2020 Modelling and nanoscale force spectroscopy of frequency modulation atomic force microscopy *Appl. Math. Model.* **79** 544–54
[60] Dagdeviren O E, Zhou C, Altman E I and Schwarz U D 2018 Quantifying tip-sample interactions in vacuum using cantilever-based sensors: an analysis *Phys. Rev. Appl.* **9** 044040
[61] Hölscher H and Schwarz U D 2007 Theory of amplitude modulation atomic force microscopy with and without Q-Control *Int. J. Non Linear Mech.* **42** 608–25
[62] Dokukin M E and Sokolov I 2012 Quantitative mapping of the elastic modulus of soft materials with HarmoniX and PeakForce QNM AFM modes *Langmuir* **28** 16060–71
[63] Raman A, Melcher J and Tung R 2008 Cantilever dynamics in atomic force microscopy *Nano Today* **3** 20–7
[64] Lin D C and Horkay F 2008 Nanomechanics of polymer gels and biological tissues: a critical review of analytical approaches in the Hertzian regime and beyond *Soft Matter* **4** 669–82
[65] Abooalizadeh Z, Sudak L J and Egberts P 2019 Nanoscale spatial mapping of mechanical properties through dynamic atomic force microscopy *Beilstein J. Nanotechnol.* **10** 1332
[66] Benaglia S, Amo C A and Garcia R 2019 Fast, quantitative and high resolution mapping of viscoelastic properties with bimodal AFM *Nanoscale* **11** 15289–97
[67] Lai C Y, Santos S and Chiesa M 2016 Systematic multidimensional quantification of nanoscale systems from bimodal atomic force microscopy data *ACS Nano* **10** 6265–72
[68] Ebeling D, van den Ende D and Mugele F 2011 Electrostatic interaction forces in aqueous salt solutions of variable concentration and valency *Nanotechnology* **22** 305706
[69] Dishon M, Zohar O and Sivan U 2009 From repulsion to attraction and back to repulsion: the effect of NaCl, KCl, and CsCl on the force between silica surfaces in aqueous solution *Langmuir* **25** 2831–6
[70] Tokuda K, Ogino T, Kotera M and Nishino T 2015 Simple method for lowering poly(methyl methacrylate) surface energy with fluorination *Polym. J.* **47** 66–70
[71] Li Y, Pham J Q, Johnston K P and Green P F 2007 Contact angle of water on polystyrene thin films: effects of CO 2 environment and film thickness *Langmuir* **23** 9785–93
[72] Worou C N, Kang J, Shen J, Yan P, Wang W, Gong Y and Chen Z 2021 Runge–kutta numerical method followed by Richardson's extrapolation for efficient ion rejection reassessment of a novel defect-free synthesized nanofiltration membrane. *Membranes* **11** 130
[73] Gauthier M, Pérez R, Arai T, Tomitori M and Tsukada M 2002 Interplay between nonlinearity, scan speed, damping, and electronics in frequency modulation atomic-force microscopy *Phys. Rev. Lett.* **89** 146104
[74] Voïtchovsky K, Giofrè D, José Segura J, Stellacci F and Ceriotti M 2016 Thermally-nucleated self-assembly of water and alcohol into stable structures at hydrophobic interfaces *Nat. Commun.* **7** 13064
[75] Foster W, Aguilar J A, Kusumaatmaja H and Voïtchovsky K 2018 *In situ* molecular-level observation of methanol vatalysis at the water–graphite interface. *ACS Appl. Mater. Interfaces* **10** 34265–71
[76] Eskelsen J R, Qi Y, Schneider-Pollack S, Schmitt S, Hipps K W and Mazur U 2014 Correlating elastic properties and molecular organization of an ionic organic nanostructure *Nanoscale* **6** 316–27
[77] Wang W, Li Z, Marsden A J, Bissett M A and Young R J 2021 Interlayer and interfacial stress transfer in hBN nanosheets *2D Mater.* **8** 035058
[78] Castellanos-Gomez A, Poot M, Amor-Amorós A, Steele G A, van der Zant H S, Agraït N and Rubio-Bollinger G 2012 Mechanical properties of freely suspended atomically thin dielectric layers of mica *Nano Res.* **5** 550–7
[79] Bertolazzi S, Brivio J and Kis A 2011 Stretching and breaking of ultrathin MoS 2 *ACS Nano* **5** 9703–9
[80] Sun Y *et al* 2019 Elastic properties and fracture behaviors of biaxially deformed, polymorphic $MoTe_2$ *Nano Lett.* **19** 761–9
[81] Pereira Júnior M L, Viana de Araújo C M, De Sousa J M, de Sousa Júnior R T, Roncaratti Júnior L F, Ferreira Giozza W and Ribeiro Júnior L A 2020 On the elastic properties and fracture patterns of MoX_2 (X = S, Se, Te) membranes: a reactive molecular dynamics study *Condens. Matter* **5** 73
[82] Zhan H, Tan X, Xie G and Guo D 2021 Reduced fracture strength of 2D materials induced by interlayer friction *Small* **17** 2005996
[83] Young's Modulus, tensile strength and yield strength values for some materials (https://engineeringtoolbox.com/young-modulus-d_417.html) 2023
[84] Chang J, Toga K B, Paulsen J D, Menon N and Russell T P 2018 Thickness dependence of the Young's modulus of polymer thin films. *Macromolecules* **51** 6764–70
[85] Zhang R, Koutsos V and Cheung R 2016 Elastic properties of suspended multilayer WSe2 *Appl. Phys. Lett.* **108** 042104
[86] Xiao J, Zhang L, Zhou K, Li J, Xie X and Li Z 2013 Anisotropic friction behaviour of highly oriented pyrolytic graphite *Carbon* **65** 53–62
[87] Falin A *et al* 2021 Mechanical properties of atomically thin tungsten dichalcogenides: WS_2 , WSe_2, and WTe_2 *ACS Nano* **15** 50

[88] Choi W R, Hong J H, You Y G, Campbell E E B and Jhang S H 2021 Suspended $MoTe_2$ field effect transistors with ionic liquid gate *Appl. Phys. Lett.* **119** 223105

[89] Chan N, Lin C, Jacobs T, Carpick R W and Egberts P 2020 Quantitative determination of the interaction potential between two surfaces using frequency-modulated atomic force microscopy *Beilstein J. Nanotechnol.* **11** 729–39

[90] Jacobs T D B, Lefever J A and Carpick R W 2015 Measurement of the length and strength of adhesive interactions in a nanoscale silicon-diamond interface *Adv. Mater. Interfaces* **2** 1400547

[91] Sader J E, Hughes B D, Huber F and Giessibl F J 2018 Interatomic force laws that evade dynamic measurement *Nat. Nanotechnol.* **13** 1088–91

[92] Huber F and Giessibl F J 2020 Experimental use of the inflection point test for force deconvolution in frequency-modulation atomic force microscopy to turn an ill-posed situation into a well-posed one by proper choice of amplitude *J. Appl. Phys.* **127** 184301

[93] Cafolla C and Voïtchovsky K 2021 Real-time tracking of ionic nano-domains under shear flow *Sci. Rep.* **11** 19540

[94] Howarth A J, Davies D L, Lelj F, Wolf M O and Patrick B O 2014 Tuning the emission lifetime in bis-cyclometalated iridium(III) complexes bearing iminopyrene ligands *Inorg. Chem.* **53** 11882–9

[95] Park J, Kim M and Kim S 2014 Surface renewable nano-iridium oxide polymeric composite pH electrodes *Sensors Actuators*B **204** 197–202

[96] Gad M M and Abualsaud R 2019 Behavior of PMMA denture base materials containing titanium dioxide nanoparticles: a literature review *Int. J. Biomater.* **2019** 190610

[97] Jin D W, Ko Y J, Kong D S, Kim H K, Ha J H, Lee M, Hong J I and Jung J H 2018 Thermal stability and Young's modulus of mechanically exfoliated flexible mica. *Curr. Appl Phys.* **18** 1486–91

[98] May P, Khan U and Coleman J N 2013 Reinforcement of metal with liquid-exfoliated inorganic nano-platelets *Appl. Phys. Lett.* **103** 163106

[99] Pan Y, Wen M, Wang L, Wang X, Lin Y H and Guan W M 2015 Iridium concentration driving the mechanical properties of iridium–aluminum compounds. *J. Alloys Compd.* **648** 771–7

[100] Material: silicon (Si), bulk (https://memsnet.org/material/siliconsibulk/) (Accessed: 30th July 2023)

[101] Zhang S X, Liu J, Zeng J, Hu P P and Zhai P F 2017 Structural modification in swift heavy ion irradiated muscovite mica *Chin. Phys.* B **26** 106102

[102] Mukhopadhyay T, Mahata A, Adhikari S and Zaeem M A 2017 Effective elastic properties of two dimensional multiplanar hexagonal nanostructures *2D Mater.* **4** 025006

[103] Ma C, Chen Y and Arnold W 2017 Detection of subsurface cavity structures using contact-resonance atomic force microscopy *J. Appl. Phys.* **121** 154301

[104] Rahman Rano B, Syed I M and Naqib S H 2020 Elastic, electronic, bonding, and optical properties of WTe_2 Weyl semimetal: a comparative investigation with $MoTe_2$ from first principles *Res. Phys.* **19** 103639

[105] Zeng F, Zhang W B and Tang B Y 2015 Electronic structures and elastic properties of monolayer and bilayer transition metal dichalcogenides MX2 (M = Mo, W; X = O, S, Se, Te): a comparative first-principles study *Chin. Phys.* B **24** 097103

[106] Properties: iridium - properties and applications (https://azom.com/properties.aspx?ArticleID=1700) (Accessed: 30th July 2023

[107] Falin A *et al* 2017 Mechanical properties of atomically thin boron nitride and the role of interlayer interactions *Nat. Commun.* **8** 15815

[108] Drelich J A R O S L A W, Tormoen G W and Beach E R 2006 Determination of solid surface tension at the nanoscale using atomic force microscopy. *Contact Angle, Wettability Adhes.* **4** 237–64

[109] Peng Q and De S 2013 Outstanding mechanical properties of monolayer MoS2 and its application in elastic energy storage *Phys. Chem. Chem. Phys.* **15** 19427–37

[110] Zhang D, Ren W, Wang K, Chen S, Zhang L, Ni Y and Zhang G 2023 A thermal conductivity switch via the reversible 2H-1T′ phase transition in monolayer $MoTe_2$. *Chin. Phys.* B **32** 050505

[111] 2023 Poisson's ratio (https://sonelastic.com/en/fundamentals/tables-of-materials-properties/polymers.html) (Accessed: 21 Sept 2023)

[112] Woo S, Park H C and Son Y W 2016 Poisson's ratio in layered two-dimensional crystals. *Phys. Rev.* B **93** 075420

[113] Castellanos-Gomez A, Poot M, Steele G A, Van Der Zant H S, Agraït N and Rubio-Bollinger G 2012 Elastic properties of freely suspended MoS_2 nanosheets *Adv. Mater.* **24** 772–5

[114] Akhter M J, Kuś W, Mrozek A and Burczyński T 2020 Mechanical properties of monolayer MoS_2 with randomly distributed defects *Materials* **13** 1307

[115] Shen J, Zhang D, Zhang F-H and Gan Y 2017 AFM tip-sample convolution effects for cylinder protrusions *Appl. Surf. Sci.* **422** 482–91

[116] Payam A F 2023 Modeling and analysis of the capillary force for interactions of different tip/substrate in AFM based on the energy method *ACS Meas. Sci. Au* **3** 194–9

[117] Bergström L 1997 Hamaker constants of inorganic materials *Adv. Colloid Interface Sci.* **70** 125–69

[118] Leite F L, Bueno C C, Da Róz A L, Ziemath E C and Oliveira O N 2012 Theoretical models for surface forces and adhesion and their measurement using atomic force microscopy *Int. J. Mol. Sci.* **13** 12773–856

[119] Fernández-Varea J M and Garcia-Molina R 2000 Hamaker constants of systems involving water obtained from a dielectric function that fulfills the f sum rule *J. Colloid Interface Sci.* **231** 394–7

[120] Ackler H D, French R H and Chiang Y M 1996 Comparisons of Hamaker constants for ceramic systems with intervening vacuum or water: from force laws and physical properties *J. Colloid Interface Sci.* **179** 460–9

[121] Lomboy G, Sundararajan S, Wang K and Subramaniam S 2011 A test method for determining adhesion forces and Hamaker constants of cementitious materials using atomic force microscopy *Cem. Concr. Res.* **41** 1157–66

[122] Kozbial A, Gong X, Liu H and Li L 2015 Understanding the intrinsic water wettability of molybdenum disulfide (MoS_2) *Langmuir* **31** 8429–35

[123] Zhang H, Ma Y, Wan Y, Rong X, Xie Z, Wang W and Dai L 2015 Measuring the refractive index of highly crystalline monolayer MoS_2 with high confidence *Sci. Rep.* **5** 8440

[124] Refractive index database. Available at: (https://refractiveindex.info/?shelf=organic&book=poly%28methyl_methacrylate%29&page=Szczurowski). (Accessed: 30th July 2023

[125] Song H, Gu H, Fang M, Chen X, Jiang H, Wang R, Zhai T, Ho Y T and Liu S 2019 Layer-dependent dielectric function of wafer-scale 2D MoS_2 *Adv. Opt. Mater.* **7** 1801250

[126] Snapp P, Kim J M, Cho C, Leem J, Haque M F and Nam S 2020 Interaction of 2D materials with liquids: wettability, electrochemical properties, friction, and emerging directions *NPG Asia Mater.* **12** 22

[127] Fatima S, Quadri S N, Parveen S, Beg S, Rahman M, Ahmad F J and Abdin M Z 2021 Polymeric nanoparticles for potential drug delivery applications in cancer *In Nanoformulation Strategies for Cancer Treatment* (Elsevier)

[128] Maiti A and Pandey A 2021 Polymer and waste plastic in membranes *Materials Science and Materials Engineering* (Elsevier)
[129] Obi B 2017 *Polymeric Foams Structure-Property-Performance: a Design Guide* (William Andrew)
[130] Aragones J L, MacDowell L G and Vega C 2011 Dielectric constant of ices and water: a lesson about water interactions *J. Phys. Chem.* A **115** 5745–58
[131] Strazdaite S, Versluis J, Backus E H G and Bakker H J 2014 Enhanced ordering of water at hydrophobic surfaces *J. Chem. Phys.* **140** 054711
[132] Seo Y, Jhe W, Katan A J, Van Es M H and Oosterkamp T H 2009 Quantitative force versus distance measurements in amplitude modulation AFM: a novel force inversion technique *Nanotechnology* **20** 9
[133] Sader J E, Uchihashi T, Higgins M J, Farrell A, Nakayama Y and Jarvis S P 2005 Quantitative force measurements using frequency modulation atomic force microscopy—theoretical foundations. *Nanotechnology* **16** S94
[134] Boer-Duchemin E, Tranvouez E and Dujardin G 2010 The interaction of an atomic force microscope tip with a nano-object: a model for determining the lateral force *Nanotechnology* **21** 455704
[135] Matei G A, Thoreson E J, Pratt J R, Newell D B and Burnham N A 2006 Precision and accuracy of thermal calibration of atomic force microscopy cantilevers *Rev. Sci. Instrum.* **77** 83703
[136] Clifford C A and Seah M P 2005 The determination of atomic force microscope cantilever spring constants via dimensional methods for nanomechanical analysis *Nanotechnology* **16** 1666
[137] Yacoot A and Koenders L 2008 Aspects of scanning force microscope probes and their effects on dimensional measurement *J. Phys. D: Appl. Phys.* **41** 103001
[138] Cafolla C, Payam A F and Voïtchovsky K 2018 A non-destructive method to calibrate the torsional spring constant of atomic force microscope cantilevers in viscous environments *J. Appl. Phys.* **124** 154502
[139] Han B, Key B, Lapidus S H, Garcia J C, Iddir H, Vaughey J T and Dogan F 2017 From coating to dopant: how the transition metal composition affects alumina coatings on Ni-rich cathodes *ACS Appl. Mater. Interfaces* **9** 41291–302
[140] Mandracci P, Mussano F, Rivolo P and Carossa S 2016 Surface treatments and functional coatings for biocompatibility improvement and bacterial adhesion reduction in dental implantology *Coatings* **6** 7
[141] Ma Y, Guo Q, Yang M, Wang Y, Chen T, Chen Q, Zhu X, Xia Q, Li S and Xia H 2018 Highly doped graphene with multi-dopants for high-capacity and ultrastable sodium-ion batteries *Energy Storage Mater.* **13** 134–41
[142] Liu Y, Huang Y and Duan X 2019 van der Waals integration before and beyond two-dimensional materials *Nature* **567** 323–33
[143] Butt H-J and Jaschke M 1995 Calculation of thermal noise in atomic force microscopy *Nanotechnology* **6** 1
[144] Snopok B, Laroussi A, Cafolla C, Voïtchovsky K, Snopok T and Mirsky V M 2021 Gold surface cleaning by etching polishing: optimization of polycrystalline film topography and surface functionality for biosensing *Surf. Interfaces* **22** 100818
[145] Bonaccurso E, Kappl M and Butt H J 2008 Thin liquid films studied by atomic force microscopy *Curr. Opin. Colloid Interface Sci.* **13** 107–19
[146] Wu W, Chen Z, Cheng X and Wang Y 2013 EBSD study of (110) orientation of iridium (Ir) coating on niobium (Nb) substrate by double glow plasma *Nucl. Instrum. Methods Phys. Res.*B **307** 315–9
[147] Voïtchovsky K, Kuna J J, Sonia Antoranz Contera E T and Stellacci F 2010 Direct mapping of the solid–liquid adhesion energy with subnanometre resolution. *Nat. Nanotechnol.* **5** 401–5